

Logical and Arithmetic Circuits in Belousov Zhabotinsky Encapsulated Discs

Julian Holley,^{1,*} Ishrat Jahan,² Ben De Lacy Costello,² Larry Bull,¹ and Andrew Adamatzky¹

¹*Faculty of Environment and Technology, University of the West of England, Bristol, England*

²*School of Life Sciences, University of the West of England, Bristol, England*

(Dated: November 19, 2021)

Excitation waves on a sub-excitable Belousov Zhabotinsky (BZ) substrate can be manipulated by chemical variations in the substrate and by interactions with other waves. Symbolic assignment and interpretation of wave dynamics can be used to perform logical and arithmetic computations. We present chemical analogs of elementary logic and arithmetic circuits created entirely from interconnected arrangements of individual BZ encapsulated cell like discs. Inter-disc wave migration is confined in carefully positioned connecting pores. This connection limits wave expansion and unifies the input-output characteristic of the discs. Circuit designs derived from numeric simulations are optically encoded onto a homogeneous photo-sensitive BZ substrate.

PACS numbers: 82.40.Ck, 89.20.Ff, 89.75.Fb, 89.75.Kd

I. INTRODUCTION

Unconventional Computing [1] is a field of study dedicated to exploring alternate computational strategies, structures and mediums contrasting contemporary digital von Neumann architecture machines [2]. Innate serial execution and storage processing of these machines presents profound throughput and energy restrictions, limiting practical application of some classes of algorithms [3]. Conversely computational capable organic adaptive systems are innately parallel and distributed. Highly parallel and distributed computation can be supported in chemical reaction-diffusion (RD) systems [4] such as the Belousov Zhabotinsky (BZ) reaction [5]. One bench mark of these systems is the ability to replicate components used in conventional computation, such as logic and arithmetic circuits. Logic gates are the physical embodiment of Boolean logic operations that form the foundation for digital computation. Circuits of logic gates can be connected to create machines capable of performing ‘*Universal Computation*’ [6].

The chemical implementation of logic gates were first described by Rossler sustained in a bistable chemical medium [7]. Logic gates have also been demonstrated using chemical kinetics [8–11]. The binary value assignment to the presence or absence of individual RD waves modulated by the substrate geometry and other waves presents an alternative approach. Toth first described logic gates with BZ waves along these lines [12, 13]. In that system RD waves travelled along thin capillary tubes. These basic principles have since led to numerous adaptations, for example Steinbock implemented logic gates by ‘printing’ a catalyst of the BZ reaction onto a facilitating medium [14]. In a simulated study Motoike presented (amongst other designs) logic gates reliant upon geometric patterns of passive diffusion boundaries embedded on an excitable field [15]. Siewiesiuk also created logical

functions from using passive diffusion lines where function arose at the intersection of perpendicular wave channels [16]. Adamatzky presented alternative logic gate designs by combining the principles of collision based computing on an precipitating chemical substrate [17, 18] and in-vitro [19]. Similar or derivations on the above studies such as: [20] using the FitzHugh-Nagumo model [21, 22] reaction, or [23] co-evolutionary system, or cardiac cell model on a GPU [24] and amongst others [25] have all implemented logic functions or gates either in simulation, in-vitro or both.

Current experiments with lipid coated vesicles of excitable media at our (and our partners [26]) laboratories have led to a novel geometric BZ mediated approach to creating logic and arithmetic functions. Representative of a 2 dimensional approximation of BZ vesicles, networks of interconnected discs containing a sub-excitable BZ formulation can be arranged to create various circuits. Logic & arithmetic circuits and polymorphic gates have been simulated in homogeneous hexagonal and orthogonal networks [27, 28] and non-homogeneous arrangements [30].

In these simulations, geometric arrangements of discs are joined together by small connecting pores. The resulting pattern modulates a homogeneous BZ Oregonator simulation grid that has adapted for monochromatic photo-sensitivity [31]. The disc boundaries are created from rings of high intensity light to emulate an impenetrable exterior membrane. Lower intensity light forms the interior disc area and connecting pores adjusted to support travelling waves.

Logically symbolic waves are able to traverse the network modulated by interaction with pathways and other waves. The disc interior can be exploited for free space collision style reactions [17] whereas the pore loci and efficiency can compartmentalise the resulting reaction [27]. Circuits have been created from logical sub assemblies in orthogonal and hexagonal networks [27, 30]. Function density can be increased by circuits that include variations in relative disc size, pore efficiency and connection angles [30]. Using this later technique we have assembled a compact elementary arithmetic circuit.

* julian2.holley@uwe.ac.uk; <http://uncomp.uwe.ac.uk/holley>

Conceivably other cell geometries (such a grids of square units) could compartmentalise the cell function similar to discs. Nevertheless, the curvature of the wave front in combination with the disc geometry provides a natural and convenient unit and network structure. In comparison to our previous free space [32] or channelled logic optically projected circuits [33] the combination of the natural positively expanding wave curvature the disc geometry promotes functional inter-disc stability and connectivity.

Use of a photo-sensitive adapted version of the Oregonator model permits a simple migration from simulation to experiment. Circuit designs from the simulation can be projected directly onto an actual photo-sensitive BZ medium. Furthermore, the same substrate is capable of supporting different successive circuits. Detected activity in assigned output discs can trigger the projection of new alternate circuits onto the same substrate area. Those triggering waves can be *captured* into the new circuit, effectively becoming inputs into the new circuit. Migration of our stabilising disc centric circuit simulations onto a reusable chemical substrate is the primary subject of this report.

II. METHODS

Designs are initially created in simulation and then the resulting geometry is then projected onto the BZ substrate. This substrate is a photo sensitive BZ system [34] with a $\text{Ru}(\text{bpy})_3^{3+}$ catalyst immobilised on silica gel [35]. The medium is oscillatory in the dark with composition [36]. Global illumination levels are manually adjusted to promote marginal excitation waves. Simultaneous multiple wave initiations are optically instigated. Removing all inhibiting light promotes mass wave excitation across the BZ substrate. Normal light levels and experimental pattern are then restored with the exception of small circular zones at desired initiation points. Wave fragments continue to emerge from these dark zones out into the marginal zone of the disc body.

A. Numerical simulation

Numerical simulations are based on a 2 variable version of the Oregonator model [37] as a model of the BZ reaction [5, 38] adapted for photo-sensitive modulation of the Ru-catalysed reaction [31].

$$\begin{aligned}\frac{\partial u}{\partial t} &= \frac{1}{\epsilon}(u - u^2 - (fv + \phi)\frac{u - q}{u + q}) + D_u \nabla^2 u \\ \frac{\partial v}{\partial t} &= u - v\end{aligned}$$

Variables u and v are the local instantaneous dimensionless concentrations of the bromous acid autocatalyst activator HBrO_2 and the oxidised form of the catalyst

inhibitor $\text{Ru}(\text{bpy})_3^{3+}$. ϕ symbolises the rate of bromide production proportional to applied light intensity. Bromide Br^- is an inhibitor of the Ru-catalysed reaction, therefore excitation can be modulated by light intensity; high intensity light inhibits the reaction. Dependant on the rate constant and reagent concentration ϵ represents the ratio of the time scales of the two variables u and v . q is a scaling factor dependent on the reaction rates alone. The diffusion coefficients D_u and D_v of u and v were set to unity and zero respectively. The coefficient D_v is set to zero because it is assumed that the diffusion of the catalyst is limited. Inputs were instigated by perturbing the activator $u = 1.0$ centrally in small circular disc areas, $rad = 2$ simulation points (SP).

Parameter	Value	Description
ϵ	0.022	Ratio of time scale for variables u and v
q	0.0002	Propagation scaling factor
f	1.4	Stoichiometric coefficient
ϕ	★	Excitability level (proportional to light level)
u	~	Activator HBrO_2
v	~	Inhibitor $\text{Ru}(\text{bpy})_3^{3+}$
D_u	1.0	Activator diffusion coefficient
D_v	0	Inhibitor diffusion coefficient
Δx	0.25	Spatial step
Δt	0.001	Time step

TABLE I. Kinetic and numerical values used in numerical simulations of (Eq. 1). ★ ϕ Varies between two levels, sub-excited ($L1$) and inhibited ($L2$), $\phi_{L1} = 0.076$, $\phi_{L2} = 0.209$

Numerical simulations were achieved by integrating the equations using the Euler-alternating direction implicit (ADI) method. method [39] with a time step $\delta t = 0.001$ and a spatial step $\delta = 0.25$. Experimental parameters are given in Tab. I.

Networks of discs were created by mapping 2 different ϕ values (proportional to light intensity) onto a rectangle of homogeneous simulation substrate. To improve simulation performance the rectangle size was automatically adapted depending on the size of the network, but the simulation point (SP) density remained constant throughout. The excitation levels, $L1 \rightarrow L2$ relate to the partially active disc interiors and non-active substrate.

Discs are always separated by a single simulation point (1 SP) wide boundary layer. Connection pores between discs are created by superimposing another small *link* disc at the point of connection (typically a 2 \rightarrow 6 SP radius), simulation points have a 1:1 mapping with on screen pixels. The reagent concentrations are represented by a red and blue colour mapping; the activator, u is proportional to red level and inhibitor, v proportional to blue. The colour graduation is automatically calibrated to minimum and maximum levels of concentration over the simulation matrix. The background illumination is mono-chromatically calibrated in the same fashion pro-

portional to ϕ , white areas are inhibitory and dark areas excited (for monochromatic reproductions, blue (v) has been suppressed and red (u) appears as light gray, colour versions online).

Wave fragment flow is represented by a series of superimposed time lapse images (unless stated otherwise), the time lapse is 50 simulation steps. To improve clarity, only the activator (u) wave front progression is recorded. Figure 1 illustrates the same wave fragment in both colour map (u & v) and final composite time lapse version (u).

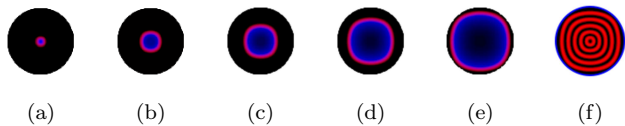


FIG. 1. (Colour online) Example the time lapse image creation. The image shown in (f) is the accumulation of successive images shown from central wave initiation in (a) to extinction in (e). Time lapses periods are 50 time steps and the refractory tail of the inhibitor (u) shown in blue (gray inner shadow of propagating ring [(a)→(e)]) is not shown in the time lapse image (f) to improve clarity.

Inputs are created by perturbing a small circular area of the activator (u) set to a value of 1.0 with a radius of $2 SP$ in the center of the disc. In addition to explicit labelling, all discs representing inputs and outputs are also highlighted with a blue and green border respectively.

In a previous study we have shown that logic circuits can be created with uniform discs arranged in hexagonal networks [29], hexagonal packing being the most efficient method of sphere (disc) packing. Further opportunities to modulate wave fragment behaviour are presented when disc size, connection angle and connection efficacy are combined in non-homogeneous networks. Disc size can be adjusted to permit or restrict internal wave interactions, producing either larger reaction vessel discs or smaller communications discs (Fig. 2a). Connection angle between discs can be used to direct wave collisions (Fig. 2b) and connection efficiency can effect the wave focus (Fig. 2c).

B. Experimental

A Sanyo proxtax multiverse projector was used to project the design outline of several simulated circuit designs from [30]. Wave activity was captured using a Lumenera infinity 2 USB 2.0 scientific digital camera. The open reactor was surrounded by a water jacket thermostatted at 20°C . Peristaltic pumps were used to pump the reaction solution into the reactor and remove the effluent (Fig. 3).

Sodium bromate, sodium bromide, malonic acid, sulphuric acid, tris(bipyridyl) ruthenium(II) chloride, 27% sodium silicate solution stabilised in $4.9M$ sodium

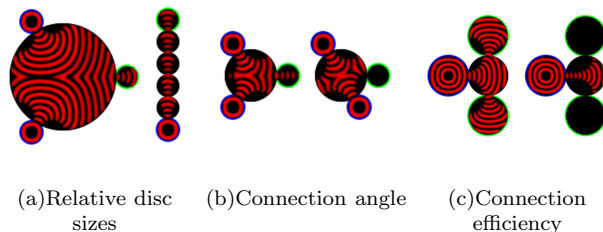


FIG. 2. (Colour online) (a) Discs as reaction vesicles in the LHS network or communication channels in the RHS network. (b) The effect of connection angle, the two input signals combine in the left network to produce an output. Adjusting the angle of the lower input in the right network alters the result of the collision and no output is produced. (c) The effect of connection efficiency. Large aperture ($6 SP$) connection in the left network results in a broad spreading beam. Conversely a smaller ($4 SP$) aperture connection in the right network creates a narrow beam wave.

hydroxide[40] and used as received unless stated otherwise. $\text{Ru}(\text{bpy})_3^{3+}$ was recrystallised from the chloridate salt with sulphuric acid. To create the catalyst loaded gels a thin layer chromatography pre-coated plates silica gel with 254nm fluorescent indicator on glass was cut into $5\text{cm} \times 5\text{cm}$ and placed in a solution of 0.9ml of $0.025M$ $\text{Ru}(\text{bpy})_3^{3+}$ and 12ml of deionised water in a Petri dish for 12 hours. Gels were washed in deionised water to remove by products before use.

The catalyst free reaction mixture was freshly prepared in a 30ml continuously-fed stirred tank reactor (CSTR), which involved the in situ synthesis of stoichiometric bromomalonic acid from malonic acid and bromine generated from the partial reduction of sodium bromate. This CSTR in turn continuously fed a thermostatted open reactor with fresh catalyst-free BZ solution in order to maintain a nonequilibrium state. The final composition of the catalyst-free reaction solution in the reactor was: $0.42M$ sodium bromate, $0.19M$ malonic acid, $0.64M$ sulphuric acid and $0.11M$ bromide. The residence time was 30 minutes.

The spatially distributed excitable field on the surface of the gel was achieved by the projection of the disc pattern from the simulations. The light intensity of discs was controlled by computer. The pattern was projected onto the catalyst loaded gel via a data projector. Every 10 seconds, a light level of $5.7\text{mW}/\text{cm}^2$ for 10ms during which time an image of the BZ fragments on the gel was captured. The purpose of this was to allow activity on the gel to be more visible to the camera. Captured images were processed to identify chemical activity. This was done by differencing successive images to create a black and white image. The images were cropped and layered to show progression of a single image finally the disc boundary was superimposed on the images to aid analysis of the results.

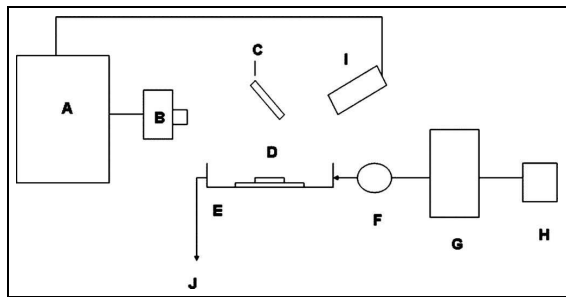


FIG. 3. Experimental setup: A light sensitive catalyst $\text{Ru}(\text{bpy})_3^{3+}$ loaded silica gel is immersed in catalyst free BZ reaction solution in a thermostatted (G) Petri dish (E). Peristaltic pump (F). Reactor with thermostatted reaction solution and to remove effluent (J). The reaction solution reservoir (H) is kept in an ice bath. The heterogeneous network on the surface of the gel (D) is constructed by the projection (B) of a disc pattern generated by a computer (A) via a mirror assembly (C). Images captured with a Digital camera fitted with a 455nm narrow bandpass interference filter (I).

III. RESULTS

We report on a selection of experiments that successfully migrated from simulation; a diode, NAND gate, XOR gate and an simple arithmetic adder circuit [30]. In the following images the inverse monochromatic wave progression (left column) is illustrated adjacent to the respective colour simulation analogue (right column). Although the parameterisation of the simulation creates different wave dynamics the projected geometry in each case is proportionally identical resulting in the same functionality.

A. Diode

The diode junction constructed with BZ discs operates by simultaneously exploiting a right angle junction and asymmetric pore size (Fig. 4). A wave fragment (y) travels horizontally from right \rightarrow left (Fig. 4a). Wave fragments cannot survive when the fragment size drops below some critical level [41]. A constricted pore of (4 SP) at the perpendicular junction reduces the wave size close to termination in the proceeding disc. Wave development is momentarily marginal before slowly recovering. Delay in wave development prohibits the fragment entering the vertical connection (Movies Mov. 1a&b [42]). Conversely the opposing vertical fragment (y) enters the junction through a broad pore (6 SP). The resultant increased junction wave seed permits the fragment to develop more rapidly and dissipate into the horizontal discs line (Fig. 4b). Therefore signal propagation only progresses from vertical to horizontal ($x \rightarrow y$). Discs in the simulation have a diameter of 56 SP which results in a projected gel disc of 10mm \varnothing . This diode junction has been used to inject a unidirectional wave fragments

into a type of simulated 1 bit memory where unidirectional waves indefinitely circulate around a loop of discs until reagent exhaustion or collision with an opposing wave [30].

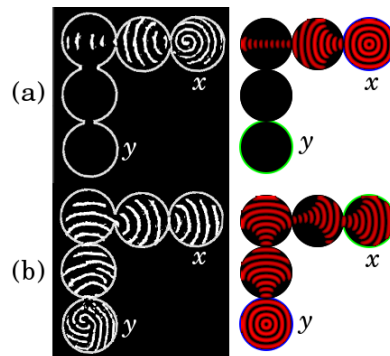


FIG. 4. (Colour online) Diode junction ($x \rightarrow y = 0$, $y \rightarrow x = 1$). Left column sequences show wave (signal) development compared alongside analogous numerical simulations on the right. (a) Signal propagates horizontally ($x \rightarrow y$). A narrow band pore (4 SP) at the 2^{nd} (right angle) junction prohibits propagation downwards to y . (b) Signal propagates vertically ($y \rightarrow x$). A broad band pore (6 SP) at the 2^{nd} (right angle) junction connection permits the signal to expand horizontally towards x . Simulation to gel projection ratio is $56\text{ SP} : 10\text{mm}$ \varnothing (Mov. 1a&b [42]).

B. NAND logic gate

A NAND gate design is shown in Fig. 5 and animated in movies Mov. 2a \rightarrow c [42]. The gate is a conjunction of an AND gate and an *inverter* or NOT gate. The NOT gates operates horizontally in the bottom four discs. A logical TRUTH or '1' (supply wave) is always presented simultaneously with the inputs x & y . In the case of $(x, y) = (0, 0)$ a wave propagates horizontally unimpeded terminating in the output disc z , ($z = 1$) (Fig. 5a). Presentation of input cases $(x, y) = (1, 0) \mid (0, 1)$ also have no effect on the progression of the supply wave and in both cases $z = 1$ (Fig. 5b). In the final instance $(x, y) = (1, 1)$ the inputs collide in the central disc resulting in a perpendicular ejection wave. The downward ejection wave fragment propagates into the horizontal NOT line below and deflects and causes the extinction of the supply wave leading to a negated output ($z = 0$) (Fig. 5c). The NAND gate is significant because of its universal applicability in the construction of all other logic gates. This design is illustrative of the modular facilitation of BZ disc networks creating a NAND gate from the conjunction of an AND and a NOT gate.

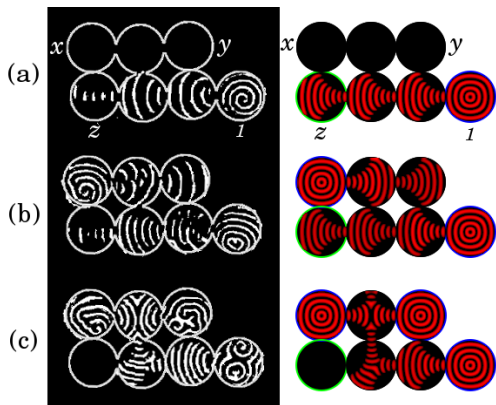


FIG. 5. (Colour online) Two input NAND gate ($z = \overline{x \bullet y}$). Left column sequences show wave (signal) development compared alongside numerical simulations on the right. (a) $z = 1, (x, y) = [0, 0]$. (b) $z = 0, (x, y) = [0, 1]$. (c) $z = 0, (x, y) = [1, 1]$. Pores of 6 SP interconnect 56 $SP\emptyset$ discs with simulation to gel projection ratio of 56 $SP : 10mm \emptyset$ (Mov. 2a \rightarrow c [42]).

C. XOR logic gate

Figure. 6 demonstrates the XOR function. As with the preceding NAND gate, a logical TRUTH ('1') is supplied in two discs (centre top and bottom right) in synchronisation with the two inputs (x & y). Presentation of $(x, y) = (0, 0)$ allows the vertical supply wave to deflect the horizontal supply wave resulting in logical false output $z = 0$ (Fig. 6.a). Complimentary inputs $(x, y) = (0, 1)$ & $(1, 0)$ deflect the vertically travelling supply wave allowing the horizontal supply wave reaching the output disc ($z = 1$) (Fig. 6.b). Finally the input presentation of $(x, y) = (1, 1)$ cancels the effect of the asymmetric collision of the vertical supply wave again deflecting the horizontal wave path ($z = 0$) (Fig. 6.c) (Mov. 3a \rightarrow c [42]).

Using this design strategy we have constructed other simulated gates (NOT, AND, OR, NXOR) and with combinations the we have also simulated simple memory and arithmetic circuits [30].

D. Composite one bit half adder circuit

One of the building blocks of electronic digital arithmetic circuits is the 1 bit half adder (HA). Two HA circuits can be connected to make a full 1 bit adder. One bit adders can then be repeated connected to make an n bit adder. A successful construction of a HA is therefore demonstrative of arithmetic capabilities of this scheme. The HA circuit takes 2 inputs; the n bit (x) in conjunction with a carry (y) and produces two outputs, the sum (S) and carry (C). A HA can be constructed from a combination of two logic gates the XOR and AND gate. There are two inputs (x & y) and two outputs (S & C), the

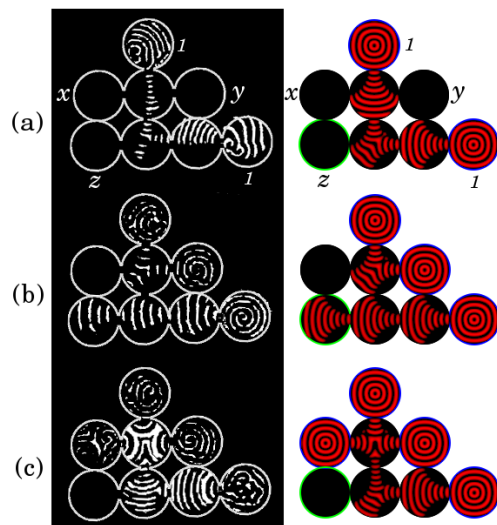


FIG. 6. (Colour online) Two input XOR gate ($z = x \oplus y$). Left column sequences show wave (signal) development compared alongside numerical simulations on the right for the input sets (a) $z = 0, (x, y) = [0, 0]$. (b) $z = 1, (x, y) = [0, 1]$ & $[1, 0]$. (c) $z = 0, (x, y) = [1, 1]$. Pores of 6 SP interconnect 56 $SP\emptyset$ discs with simulation to gel projection ratio of 56 $SP : 10mm \emptyset$ (Mov. 3a \rightarrow c [42]).

binary sum (S) of x & y is achieved by the XOR gate ($S = x \oplus y$) and inability of the configuration (overflow) to present the $1 + 1$ input is achieved with a carry (C) output, ($C = x \bullet y$).

We have conceived several simulated half adders and full adders circuits arranged in orthogonal [30] and hexagonal [27] networks where AND & XOR gates form building blocks in a larger circuit. Nevertheless it is possible to increase functional density by adding flexibility. With the exception of the previous diode, the above logic gates are constructed with discs connected with a uniform orthogonal network and connection pores. More efficient designs are possible by permitting flexibility in terms of disc size, connection pore (see diode) and inter disc connection angle.

Figure 7 illustrates a compact HA circuit design where the XOR & AND gate are combined in a central single reactor disc (R). Interconnecting discs ($r1, r2$) between the central reactor disc guide wave fragments to the S output to create the XOR feature ($xy(1, 0)$ & $xy(0, 1) \rightarrow S = 1, C = 0$). The AND feature is created by the perpendicular wave ejection fragments directly into the (C) ($xy(1, 1) \rightarrow S = 0, C = 1$) (Mov. 4a&b [42]).

IV. DISCUSSION

In much the same way that electronic circuits are designed and constructed we have created an alternative HA circuit to that presented above. In that instance the HA circuit is formed from the conjunction of an AND gate unit and a XOR gate unit. Recursive connections too have led

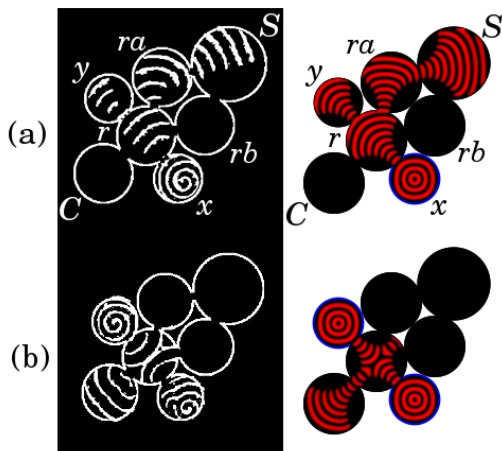


FIG. 7. (Colour online) One bit half adder circuit ($S = x \oplus y$, $C = x \cdot y$). The central reactor disc perform both XOR and AND logic functions to create the desired logic. (a) XOR component, $S = 1$, $C = 0$, $(x, y) = [0, 1][1, 0]$. (b) AND component, $S = 0$, $C = 1$, $(x, y) = [1, 1]$. Pores of 4 SP interconnect discs $56 SP \varnothing$ disc, scaled by 1.2 for S and 0.8 for $x \& y$ with simulation to gel projection ratio of $56 SP:10mm \varnothing$. The circuit exploits 3 types of wave modulation, connection angle, disc size and pore efficacy) (Mov. 4a&b [42]).

to the creation of memory and sequential circuits that can be combined with diodes and logic gates to create other circuits. Beyond the limitations of our own laboratory resources we foresee no reason preventing successful migration of these additional circuits.

Although these circuits share some similarity to their electronic counterparts, there are differences. Reagents, the chemical analog of the *power supply* is embedded and distributed throughout the circuit substrate and not supplied from one source. A circuit can thus activate for short periods in absence of any reagent refreshment. The vector component of the reaction wave presents another interesting contrast. Temporally separated waves can share a common channel without interference. It is therefore possible to create a ‘cross-roads’ junction where wave signals travelling in different directions can share the same substrate without interference [30]. Furthermore the optical circuit projection onto a homogeneous substrate permits substrate reuse with preservation current signals. One operating circuit projection can be instantaneously replace with another circuit. Waves in target locations could trigger circuit changes and conceivably also incorporate other existing wave signals into the *new* circuit.

At a scale where excitation waves are visible with the human eye this (BZ) reaction diffusion process is relatively slow. In these experiments discs are $\sim 10mm$ in diameter and waves propagate at approximately $\sim 0.5mms^{-1}$ resulting in a $20s$ propagation delay per disc. Wave front geometry is an emergent property of the chemical composition and substrate, that develops independently to the initiation geometry. Reducing the

disc physical dimensions therefore requires an proportionate increase in chemical kinetics to maintain functional equilibrium. For example; if the chemical kinetics could be adapted to reduce the wave front size, then a reduction in diameter to that of a typical neuron from ($10mm \rightarrow 0.004mm$) could at least produce a linear adjustment in disc propagation delay $20/2500 = 8ms$; in comparison the refractory phase of a typical neuron is $\sim 1ms$.

This research is an exploratory component within a wider collaborative project that aims to create functional networks of lipid encapsulated BZ vesicles [26]. The lipid membrane and the non-linear oscillatory nature of the BZ medium encodes some of the features apparent in biological information processing; there are systematic analogies between electro-biochemical neurons and BZ discs, such as pores \rightarrow synapses and chemical \rightarrow electrical excitation and refraction.

V. FUTURE WORK

To demonstrate the computational abilities of BZ encapsulated discs we have combined Boolean information representation and geometric collision style manipulation. The essential components required for a universal computer could be created with this combination. Nevertheless other modes of information representation and manipulation are possible in these networks. In an oscillatory mode, information could be coded in pulse phase relationships and manipulated by interconnected temporal associations, reminiscent of natural neural information processing. Information is processed probabilistically along the edge of the BZ instability threshold through interconnected membrane pores. Larger reactor chambers could possibly be connected by strings of smaller discs or vesicles.

Our explorations have so far been restricted in 2 dimensions. Discs have been substituted for cross sections of interconnected vesicles. In future studies we plan to extend our simulations into the third dimension. We speculate that similar modulation of wave *cones* could also be possible leading to 3D vesicle computational or adaptive circuits.

Designing anything beyond all but the simplest devices in such schemes as is the case with neural networks, can be uncertain and complex. We intend to create discs capable of adaptation in order to learn solutions as well as employing evolutionary strategies to search for static structural solutions. Currently we are exploring an evolutionary strategy to replicate the functionality of our manual designs of logic gates and arithmetic circuits. Success there opens the possibility on solving computational tasks for which solutions are currently protracted in conventional systems.

VI. CONCLUSION

Concomitant within our long term project aims we have developed a prototype information processing system from interconnected arrangements of BZ encapsulated discs as analogs of BZ vesicles. Expanding excitation waves sustained in a sub-excitable BZ substrate represent discrete quanta of information. The interconnecting disc pores have a stabilising effect on the waves as they propagate from one disc to another. Connections, pore efficiency, connection angle and relative disc size are used to manipulate waves to create explicit chemical information processing devices.

Networks of these units share some features apparent in biological information processing. Whilst inter-neuron communication is predominately electrical, modulation

of that activity is chemical. In the case of individual neurons modulation dominates at the synaptic junction. The membrane pore between two vesicles can be considered a simple analog of the synapse, a small contact area that can modulate signals in between vesicles. Similarly the electric upstate firing and downstate quiescence of neural signalling is an analogue of chemical excitation and refraction.

VII. ACKNOWLEDGEMENTS

This work is funded under 7th FWP FET European project 248992. We thank the project coordinator Peter Dittrich and project partners Jerzy Gorecki & Klaus-Peter Zauner for their inspirations and useful discussions [26]. The authors also acknowledge the EPSRC grant no. EP/E016839/1 for support of Ishrat Jahan.

-
- [1] *Unconventional Computing 2007*, edited by A. Adamatzky, B. De Lacy Costello, L. Bull, S. Stepney, and C. Teuscher (Luniver Press, 2006).
- [2] *John von Neumann: Selected Letters*, edited by M. Rédei (American Mathematical Society, London, 2005).
- [3] D. Harel, *Computers Ltd what they really can't do* (OUP, Oxford, England, 2003).
- [4] A. Adamatzky, B. De Lacy Costello, and T. Asai, *Reaction-Diffusion Computers* (Elsevier Science Inc., New York, 2005).
- [5] A. M. Zhabotinsky and A. N. Zaikin, *Journal of Theoretical Biology* **40**, 45 (1973).
- [6] A. Turing, *Proceedings of the London Mathematical Society* **42**, 230 (1936).
- [7] O. E. Rossler, in *Physics and mathematics of the nervous system*, edited by M. Conrad, W. Guttinger, and M. Dal (Springer, Berlin, 1974) pp. 399–418.
- [8] A. Hjelmfelt, E. D. Weinberger, and J. Ross, *Proceedings of the National Academy of Sciences of the United States of America* **88**, 10983 (Dec 1991).
- [9] A. Hjelmfelt, E. D. Weinberger, and J. Ross, *Proceedings of the National Academy of Sciences of the United States of America* **89**, 383 (Jan 1992).
- [10] A. Hjelmfelt, E. D. Weinberger, and J. Ross, *Science* **260**, 335 (April 1993).
- [11] M. O. Magnasco, *Phys. Rev. Lett.* **78**, 1190 (Feb 1997).
- [12] A. Tóth, V. Gaspar, and K. Showalter, *The Journal of Physical Chemistry* **98**, 522 (1994).
- [13] A. Tóth and K. Showalter, *Journal of Chemistry Physics* **103**, 2058 (1995).
- [14] O. Steinbock, A. Toth, and K. Showalter, *Science* **267**, 868 (1995).
- [15] I. Motoike and K. Yoshikawa, *Phys. Rev. E* **59**, 5354 (May 1999).
- [16] J. Siewiesiuk and J. Górecki, *The Journal of Physical Chemistry A* **105**, 8189 (2001),.
- [17] A. Adamatzky and B. De Lacy Costello, *Phys. Rev. E* **66**, 046112 (Oct 2002).
- [18] A. Adamatzky, *Chaos, Solitons & Fractals* **21**, 1259 (2004).
- [19] B. De Lacy Costello and A. Adamatzky, *Chaos, Solitons & Fractals* **25**, 535 (2005).
- [20] I. N. Motoike and A. Adamatzky, *Chaos, Solitons & Fractals* **24**, 107 (2005).
- [21] R. FitzHugh, *Biophysical Journal* **1**, 445 (1961).
- [22] J. Nagumo, S. Arimoto, and S. Yoshizawa, *Proceedings of the IRE* **50**, 2061 (Oct. 1962).
- [23] C. Stone, R. Toth, B. De Lacy Costello, L. Bull, and A. Adamatzky, in *Parallel Problem Solving from Nature PPSN X*, Lecture Notes in Computer Science, Vol. 5199, edited by G. Rudolph, T. Jansen, S. Lucas, C. Poloni, and N. Beume (Springer Berlin / Heidelberg, 2008) pp. 579–588.
- [24] S. Scarle, *Computational Biology and Chemistry* **33**, 253 (2009).
- [25] J. Górecki and J. N. Górecka, in *Encyclopedia of Complexity and Systems Science*, edited by R. A. Meyers (Springer-Verlag, 2009).
- [26] NeuNeu, “Artificial wet neuronal networks from compartmentalised excitable chemical media project,” <http://neu-n.eu> (2010).
- [27] A. Adamatzky, B. De Lacy Costello, L. Bull, and J. Holley, *Israel Journal of Chemistry* **51**, 1 (2011).
- [28] A. Adamatzky, B. De Lacy Costello, and L. Bull, *International Journal of Bifurcation and Chaos*, (in press)(2011).
- [29] A. Adamatzky, J. Holley, L. Bull, and B. De Lacy Costello, *Chaos, Solitons & Fractals* (in press)(2011).
- [30] J. Holley, A. Adamatzky, L. Bull, B. De Lacy Costello, and I. Jahan, *Nano Communication Networks* **2**, 50 (2011).
- [31] L. Kuhnert, *Nature* **319**, 393 (1986).
- [32] B. De Lacy Costello and A. Adamatzky, *Chaos, Solitons and Fractals* **25**, 535 (2005).
- [33] B. De Lacy Costello, A. Adamatzky, I. Jahan, and L. Zhang, *Chemical Physics* **381**, 88 (2011).
- [34] V. Gáspár, G. Bazsa, and M. T. Beck, *Z. Phys. Chem. (Leipzig)* **264**, 43 (1983).
- [35] J. Wang, S. Kádár, P. Jung, and K. Showalter, *Phys. Rev. Lett.* **82**, 855 (1999).

- [36] Solution of catalyst free BZ medium :- $\text{NaBrO}_3 = 0.36M$,
 $\text{CH}_2(\text{COOH})_2 = 0.0825M$, $\text{H}_2\text{SO}_4 = 0.18M$,
 $\text{BrMA} = 0.165M$ & catalyst concentration @ $0.004M$.
- [37] R. M. Noyes, R. Field, and E. Koros, *Journal of the American Chemical Society* **94**, 1394 (Feb 1972).
- [38] A. N. Zaikin and A. M. Zhabotinsky, *Nature* **225**, 535 (1970).
- [39] W. H. Press, B. P. Flannery, S. A. Teukolsky, and W. T. Vetterling, *Numerical Recipes in C: The Art of Scientific Computing*, 2nd ed. (Cambridge University Press, England, 1992).
- [40] Purchased from Aldrich (U.K.).
- [41] T. Kusumi, T. Yamaguchi, R. R. Aliev, T. Amemiya, T. Ohmori, H. Hashimoto, and K. Yoshikawa, *Chemical Physics Letters* **271**, 355 (1997).
- [42] See EPAPS Document No. E-xxxxxx-xx-Rxxxxx supplementary movies. For more information on EPAPS, see <http://www.aip.org/pubservs/epaps.html>.